

Structure, Raman, and photoluminescence properties of SnO₂/MgO core-shell nanowires

Hoon Huh^a, No-Hyung Park^a, Han Gil Na^b, Dong Sub Kwak^b, Jinho Ahn^b, Heon Ham^c, Kwang Bo Shim^b, Changhwan Choi^b, Joon-Hyuk Chang^d, Chongmu Lee^e, Inpil Kang^f, Myung Ho Kong^g, Dae-Sup So^h, Joon Woo Leeⁱ, Hyoun Woo Kim^{b,*} and Kyoung Hun Kim^j

^aKorea Institute of Industrial Technology, 35-3 HongCheon-ri, Ipjang-myeon, Seobuk-gu, Cheonan-si, 331-825, Republic of Korea

^bDivision of Materials Science and Engineering, Hanyang University, Seoul 133-791, Republic of Korea

^cH & H Co. LTD, Chungju National University, 50 Daehak-ro, Chungju-si, Chungbuk, 330-702, Republic of Korea

^dSchool of Electronic Engineering, Hanyang University, Seoul 133-791, Republic of Korea

^eDivision of Materials Science and Engineering, Inha University, Incheon 402-751, Republic of Korea

^fDepartment of Mechanical and Automotive Engineering, Pukyong National University, Busan 608-739, Republic of Korea

^gKorea Institute of Materials Science, Changwon, Gyeongnam 641-831, Republic of Korea

^hNational Nanotechnology Policy Center, Korea Institute of Science and Technology Information, Seoul 130-741, Republic of Korea

ⁱDepartment of Technology Commercialization Information, KISTI, Seoul 130-741, Republic of Korea

^jKorea Institute of Ceramic Engineering and Technology, Seoul 153-801, Korea

We prepared MgO-coated SnO₂ nanowires, by means of fabricating SnO₂ core nanowires and subsequently evaporating an MgB₂ powder onto the core nanowires. We investigated changes in the morphological, structural, Raman, and photoluminescence (PL) characteristics resulting from application of the coating process and of a thermal annealing process. The surface of the nanowires became roughened by the MgO coating. While the core nanowires corresponded to the tetragonal rutile SnO₂ structure, the shell was comprised of the cubic MgO phase. Raman spectra revealed that the core-shell nanowires exhibited a weak line for MgO-associated with surface phonon modes in a TO-LO phonon gap, in addition to the SnO₂-related lines. The room-temperature PL spectrum of core SnO₂ nanowires exhibited a 2.1 eV-centered broad band and the peak position was invariant not also by the shell coating but also by the subsequent thermal annealing. The PL intensity was increased by the MgO coating, being attributed to a diffusion effect. The PL reduction by the subsequent thermal annealing is ascribed to oxygen incorporation into the SnO₂ core nanowires.

Key words: Nanowires, SnO₂/MgO, Transmission electron microscopy (TEM), Raman, Photoluminescence.

Introduction

Tin oxide (SnO₂) is an important and inexpensive semiconductor with a wide band gap ($E_g = 3.62$ eV, at room temperature). It is well known for its potential applications in gas sensors [1], transparent conducting electrodes [2], flat display devices [3] and solar cells [4]. Accordingly, SnO₂ nanowires have been fabricated by means of a variety of techniques including redox reactions [5], laser ablation [6], and vapor-liquid-solid (VLS) catalytic growth [7]. On the other hand, magnesium oxide (MgO) is a typical wide-band-gap insulator and it can be used in a variety of area such as catalysis, additives in refractories, paints and superconductor products, and as substrates for thin film growth [8, 9]. Based on the extraordinary physical and chemical properties of the oxides SnO₂ and MgO, we expect

that nanowire heterostructures consisting of these materials will find a variety of applications.

Among a variety of nanostructures for nanodevice applications [10-19], the nanowire, which is a one-dimensional form of a nanostructure, has received a tremendous amount of attention. In particular, coaxial heterostructured nanowires have been developed for a diverse range of applications. For example, ZnO/SnO₂ core-shell nanowire sensors exhibit a drastic enhancement in NO₂ gas sensing properties compared to that of the bare ZnO nanowires [20]. SnO₂/V₂O₅ core-shell nanowires showed a significant enhancement of photocatalytic activity than bare V₂O₅ nanowires [21]. Pt/ SnO₂ core-shell nanowires have a remarkably enhanced ethanol gas- and photon-sensing properties due to the surface functionalization resulting from the formation of heterostructures [22]. Also, we have obtained an enhanced near-band-emission from ZnO/SnO₂ core-shell nanowires [23]. In regard to the MgO shell, ZnO/MgO core-shell nanowires showed substantial solar-cell efficiency improvements compared with pristine ZnO

*Corresponding author:

Tel : +82-10-8428-0883

Fax: +82-2-2220-0389

E-mail: hyounwoo@hanyang.ac.kr

nanowires [24]. Also, the MgO shell was reported to enhance the photoluminescence (PL) properties of ZnO core-shell nanowires [25].

Since both MgO and SnO_2 have extraordinary physical and chemical properties, we expect that nanowire heterostructures consisting of these materials will provide a variety of applications such as in nanoscale optoelectronics, sensors, and catalysts, etc. It has been observed that the flat-band potentials of SnO_2 nanoparticles shifted negatively once they were coated with a thin insulating MgO layer [26]. Coating of a MgO layer on SnO_2 resulted in an increase in the photocatalytic activity of SnO_2 [27]. Although dye-sensitized solar cells based only of SnO_2 are prone to a severe recombination loss, cells made of SnO_2/MgO films deliver reasonably high efficiencies [28].

In the present study, we have synthesized SnO_2/MgO core-shell nanowires, by thermal evaporation of MgB_2 powder on pre-synthesized SnO_2 nanowires. Subsequently, we have carried out thermal annealing at $800\text{ }^\circ\text{C}$, which is a high enough temperature for ultra-large-scale-integration processes, and investigated the structural, Raman, and PL properties. In a previous study, we have fabricated MgO/SnO_2 core-shell nanowires and investigated their Raman spectra [29]. To the best of our knowledge, this is the first report on the fabrication of MgO/SnO_2 core-shell nanowires and on the annealing effects of SnO_2/MgO core-shell structures.

Experimental

SnO_2 core nanowires were synthesized in a quartz tube (diameter : 55 mm). Details of the experimental apparatus have been described elsewhere [30]. The source material was pure Sn powder. We employed Au-coated Si substrates. In order to fabricate the Au-coated Si substrates, we used Si as the starting material onto which a layer of Au (about 3 nm thick) was deposited using sputtering. On top of an alumina boat with the source material, a piece of the substrate was placed with the Au-coated side downwards. The quartz tube was inserted into a horizontal tube furnace. In the heating process at $900\text{ }^\circ\text{C}$ for 1 h, the typical partial pressure percentage of O_2 and Ar partial pressure, respectively, were set to approximately at 3 and 97 %.

Coating of these SnO_2 nanowires with MgO shell layers was also achieved using the evaporation method. On top of an alumina boat with the MgB_2 powders, a piece of the SnO_2 nanowires-grown substrate was placed with the deposition side downwards. In the heating process at $900\text{ }^\circ\text{C}$, the typical partial pressure percentage of O_2 and Ar partial pressure, respectively, were set to approximately at 3 and 97% [31]. In the subsequent step, for some selected samples, a thermal annealing was performed in a quartz tube at $800\text{ }^\circ\text{C}$ for 10 minutes.

The collected product was characterized by a field emission scanning electron microscope (FE-SEM) (Hitachi, S-4200), transmission electron microscopy (TEM) (Philips, CM-200) with an attached energy dispersive X-ray spectroscope

(EDX), and X-ray diffraction (XRD) (Philips X'pert MRD diffractometer with $\text{CuK}\alpha_1$ radiation). A PL spectrum was collected by illuminating with a 325 nm wavelength from a He/Cd laser (Kimon, 1K, Japan).

Results and Discussion

Figs. 1(a) and (b) show SEM images of SnO_2 nanowires before and after the coating with MgO , respectively. Although the surface became rougher by the coating process, it is noteworthy that the 1D-nature of the product has been maintained. Fig. 2(a) shows an XRD pattern of the as-synthesized SnO_2 nanowires. The peaks are consistent with the standard JCPDS card of tetragonal SnO_2 (No. 41-1445). The XRD spectrum of MgO -coated SnO_2 nanowires prior to thermal annealing is presented in Fig. 2(b). Some of its diffraction peaks are maybe assigned to tetragonal SnO_2 (JCPDS No. 41-1445), whereas other peaks correspond to the diffraction of cubic MgO (JCPDS 45-0946).

Fig. 3(b) shows a lattice-resolved TEM image enlargement of an area near the core-shell interface of the low magnification image shown in Fig. 3(a). In the core region, the interplanar spacings between the two neighboring fringes coincide with the interplanar distance of the planes

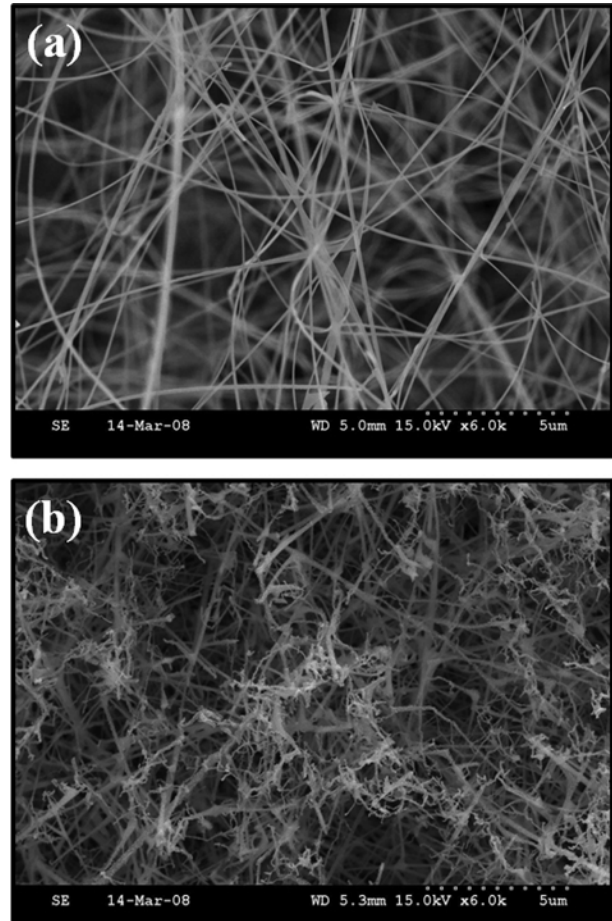


Fig. 1. SEM images of (a) core SnO_2 nanowires, (b) MgO -coated SnO_2 nanowires prior to thermal annealing.

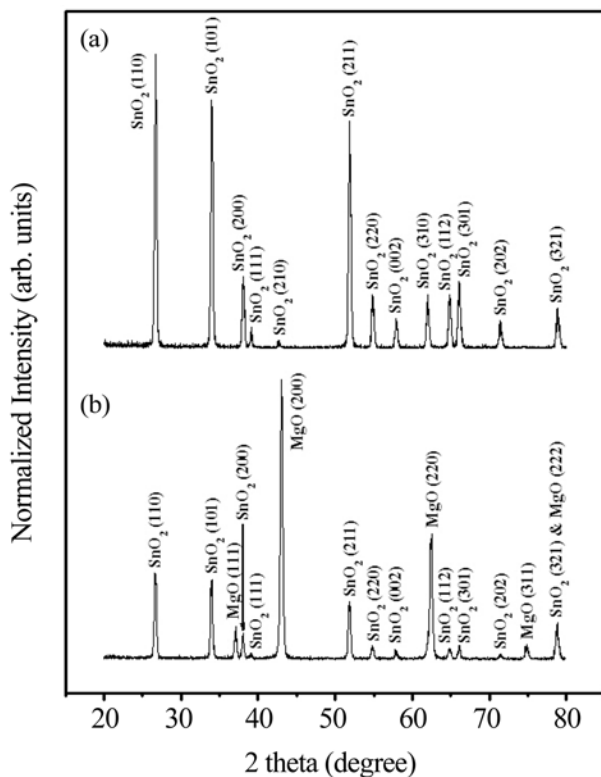


Fig. 2. XRD patterns of (a) core SnO_2 nanowires, (b) MgO -coated SnO_2 nanowires prior to thermal annealing.

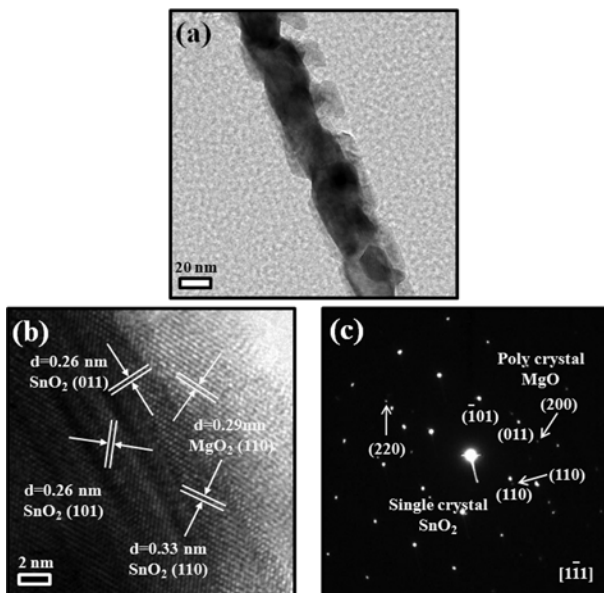


Fig. 3. (a) Lattice-resolved TEM image of a boundary region between SnO_2 -core and MgO shell layer. (b) Corresponding SAED pattern

of the tetragonal SnO_2 lattice. In the shell region, the interplanar spacing between the two neighboring fringes is about 0.29 nm, agreeing with the interplanar distance of the (110) plane of the cubic MgO lattice. Fig. 3(c) shows a corresponding SAED pattern. This exhibits not only a spot pattern of the tetragonal SnO_2 phase (JCPDS card :

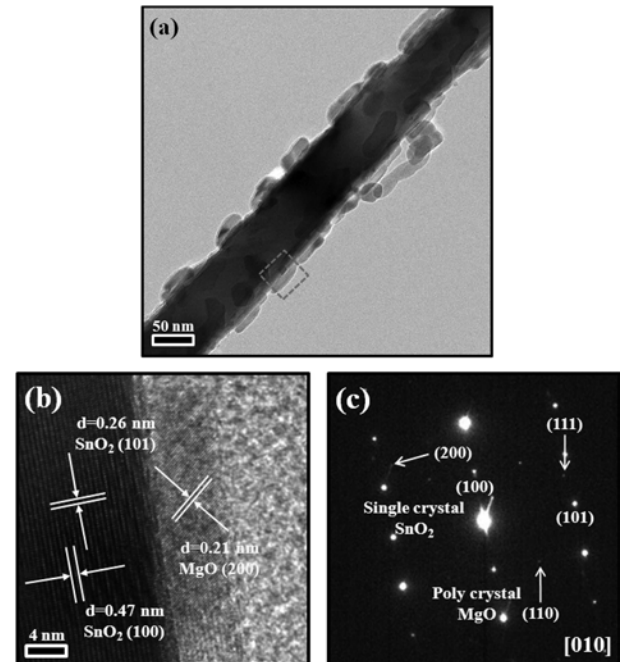


Fig. 4. (a) Low-magnification TEM image of an annealed MgO/SnO_2 core-shell nanowire, (b) Lattice-resolved TEM image enlarging an area enclosed by the square box in (a), (c) The SAED pattern shows that the annealed product is composed of amorphous and crystalline phases.

No. 41-1445), but also diffraction rings of the cubic MgO phase (JCPDS card : No. 45-0946). The spotty pattern of SnO_2 reveals a single crystal nature, whereas MgO ring spots correspond to a polycrystalline nature.

On the other hand, Fig. 4(a) shows a low-magnification TEM image of an annealed core/shell nanowire. It is noteworthy that the MgO structure has aggregated and thus some part of MgO/SnO_2 interface has been exposed to the air ambient. Fig. 4(b) is a lattice-resolved TEM image enlarging a boxed region of Fig. 4(a). While the core region is comprised of a crystalline SnO_2 phase, the shell exhibits the lattice fringes corresponding to the interplanar distance of the (200) plane of the cubic MgO lattice. Fig. 4(c) shows the associated SAED pattern. The single-crystal diffraction spots were indexed as tetragonal SnO_2 , including (100) and (101) reflections. In addition, diffraction spots consisting of the diffraction rings of cubic MgO can be observed.

Fig. 5(a) shows the Raman spectrum of core SnO_2 nanowires. The fundamental Raman scattering peaks were noticeably observed at 633 cm^{-1} and 771 cm^{-1} , corresponding to the A_{1g} and B_{2g} vibration modes in the rutile SnO_2 structure, respectively [32-35]. Fig. 5(b) shows the Raman spectrum of the as-prepared SnO_2 -core/ MgO -shell nanowires. In addition to the three Raman lines at 474 , 632 , and 774 cm^{-1} , being assigned to E_g , A_{1g} , and B_{2g} modes, respectively, a weak Raman peak at about 694 cm^{-1} was observed. It has been suggested that this line corresponds to IR-active A_{2u} LO mode [32]. On the other

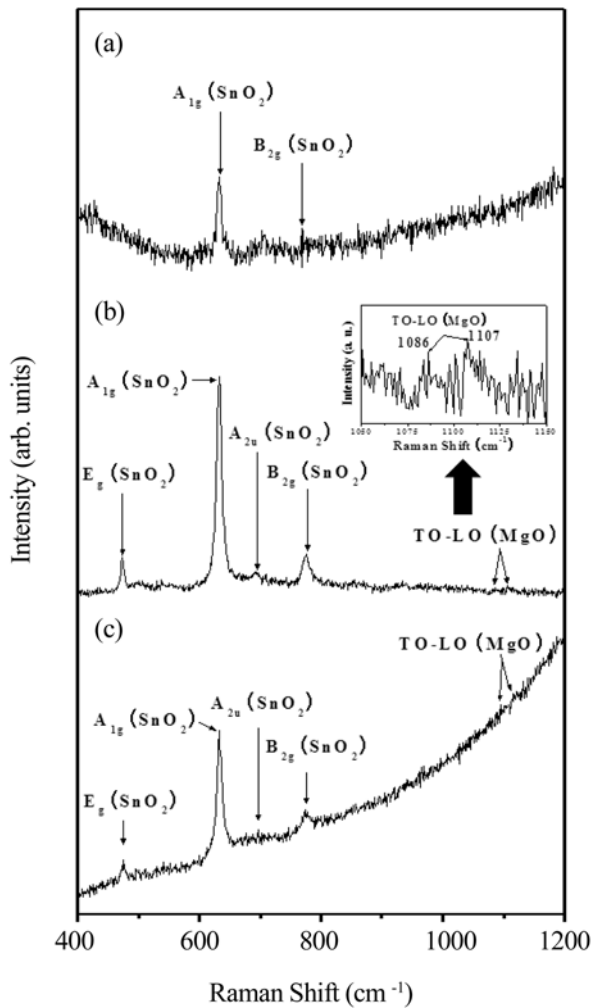


Fig. 5. Raman spectra of (a) core SnO_2 nanowires, (b) as-prepared SnO_2 -core/ MgO -shell nanowires, and (c) annealed SnO_2 -core/ MgO -shell nanowires. Insets in (b) represents the enlarged spectrum in the spectra range of $1050\text{--}1150\text{ cm}^{-1}$.

hand, the line at 1086 cm^{-1} accompanied by a line at 1107 cm^{-1} can be observed. Since these lines are very weak, we have enlarged it for clarity (upper-right inset in Fig. 5(b)). The broad band composed of two lines is similar to those observed from MgO microcrystals [36, 37], being attributed to the surface phonon modes in a TO-LO phonon gap. Fig. 5(c) shows the Raman spectrum of the annealed SnO_2 -core/ MgO -shell nanowires. Three fundamental Raman peaks at 475 , 632 , and 774 cm^{-1} , being associated with the E_g , A_{1g} , and B_{2g} modes, respectively, are found, confirming the existence of the rutile SnO_2 phase. Although their intensities are relatively weak, Raman lines at 1088 cm^{-1} and 1121 cm^{-1} , presumably from the MgO shell, were observed. By comparing Fig. 5(c) with Fig. 5(b), we reveal that the relative intensity of the IR-active LO A_{2u} mode line to the A_{1g} line was reduced by the thermal annealing. The Raman activity of the IR-active LO A_{2u} mode line is induced by disorder [33] or size effects [38]. Since the size of the core SnO_2 nanowires will not be significantly varied by the thermal annealing, we surmise that the thermal annealing

tended to decrease the disorder by increasing the crystallinity of SnO_2 core nanowires. Further study is in progress. The measured FWHM values of the A_{1g} line of core SnO_2 nanowires, as-prepared SnO_2 -core/ MgO -shell nanowires, and annealed SnO_2 -core/ MgO -shell nanowires are 8.0 , 10.3 , and 10.5° , respectively, indicating that the A_{1g} mode has been significantly broadened by the MgO -coating. We surmise that the SnO_2 nanowires tend to gain more defects such as vacancies of oxygen and vacancy clusters, during the heating process for the MgO -coating [39].

Fig. 6 shows the room-temperature PL spectra of core SnO_2 nanowires, as-prepared SnO_2 -core/ MgO -shell nanowires, and annealed SnO_2 -core/ MgO -shell nanowires. The spectra exhibited a strong and broad peak centered around 2.1 eV for all samples. In the spectrum of core SnO_2 nanowires, the 2.1 eV -peak in the yellow region originated from the defect energy levels within the bandgap of SnO_2 , being associated with O vacancies or Sn interstitials [40–42]. By means of the MgO coating, the intensity of the PL spectrum has been increased, whereas the peak position is almost invariant. Although MgO is known to exhibit blue or blue-green emissions [43], there has been a rare report on the yellow emission. Accordingly, the MgO shell does not contribute to the annealing-induced intensification of PL of the composite nanowires. During the MgO coating, at a high temperature of $900\text{ }^\circ\text{C}$, there should be an atomic diffusion near the SnO_2 -core/ MgO -shell boundaries.

The free energies of formation (ΔG_f) at the growth temperature of $900\text{ }^\circ\text{C}$ for SnO_2 and MgO are about -337 and -473 kJ/mol , respectively [44]. There exists a considerable amount of oxygen vacancies in both SnO_2 and MgO phases. Since the formation of MgO is more favorable than that of SnO_2 , oxygen atoms tend to move from the SnO_2 phase to the MgO phases (Fig. 7(a)). Accordingly, it is likely that additional oxygen vacancies are generated in the SnO_2 phase during the MgO -coating process at $900\text{ }^\circ\text{C}$. By means of thermal annealing at $800\text{ }^\circ\text{C}$, the PL intensity was slightly decreased (Fig. 6). We have used a furnace with an ambient nearly equal to air, which should

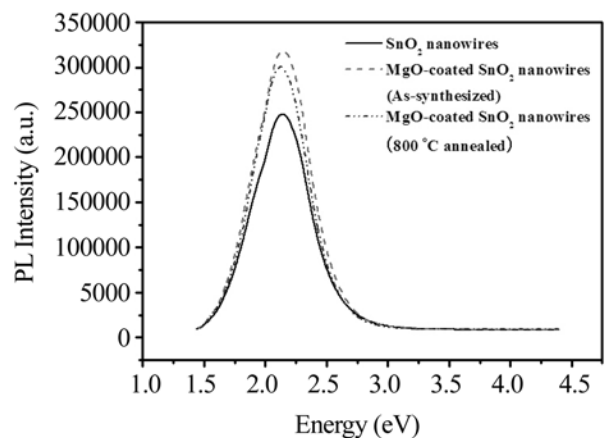


Fig. 6. PL spectra of core SnO_2 nanowires, as-prepared SnO_2 -core/ MgO -shell nanowires, and annealed SnO_2 -core/ MgO -shell nanowires.

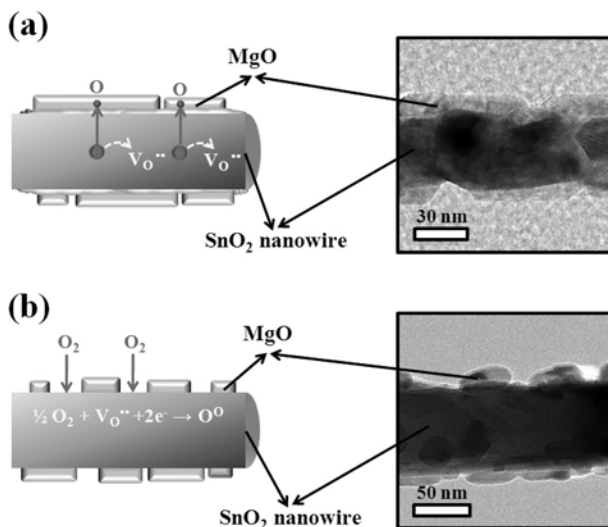


Fig. 7. Schematic outlines of the behavior of oxygen vacancies during the process for (a) MgO coating and (b) subsequent thermal annealing.

have substantial amounts of oxygen. Figs. 4(a) and 7(b) indicate that some part of MgO/SnO₂ interface has been exposed to the air ambient, during the thermal annealing. We surmise that the thermal annealing increases the density of oxygen vacancies or Sn interstitials in the SnO₂ core, intensifying the yellow emission. Although it is possible that some of oxygen atoms migrate into the MgO phase and thus generate oxygen vacancies in the SnO₂ core, we surmise that the direct incorporation of oxygen from the air ambient onto the exposed SnO₂ surface plays a crucial role in decreasing the oxygen vacancies in SnO₂ core nanowires.

Conclusions

We have prepared MgO-coated SnO₂ nanowires and subsequently investigated the effects of thermal annealing. SEM images indicate that the surface of the nanowires became rougher by the MgO coating. XRD investigation reveals that the core-shell nanowires exhibited cubic MgO-related diffraction peaks from the shell, as well as tetragonal SnO₂-related peaks from the core. SAED patterns and lattice-resolved TEM images reveal that the shell layer comprises a crystalline MgO phase, regardless of whether the samples were annealed or not. Raman spectra indicate that the core-shell nanowires exhibited a weak line for MgO-related surface phonon modes in a TO-LO phonon gap, as well as SnO₂-related lines. While the PL spectrum of core SnO₂ nanowires exhibits a yellow emission around 2.1 eV, the subsequent MgO coating did not change the peak position but enhanced the PL intensity, due to the diffusion of oxygen from SnO₂ to MgO phases and generation of oxygen vacancies in the SnO₂ phase. The subsequent thermal annealing decreased the intensity, due to the incorporation of oxygen from the annealing ambient and reduction of the oxygen vacancies in the SnO₂ core.

Acknowledgements

This work was supported by the research fund of Hanyang University (HY-2011-201100000000434).

References

- E.R. Leite, I.T. Weber, E. Longo and J.A. Varela, *Adv. Mater.* 12 (2000) 966-968.
- Y.S. He, J.C. Campbell, R.C. Murphy, M.F. Arendt and J.S. Swinnea, *J. Mater. Res.* 8 (1993) 3131-3134.
- S.J. Laverty and P.D. Maguire, *J. Vac. Sci. Technol. B* 19 (2001) 1-6.
- S. Ferrere, A. Zaban and B.A. Gregg, *J. Phys. Chem. B* 101 (1997) 4490-4493.
- Y. Liu, C. Zheng, W. Wang, Y. Zhan and G. Wang, *J. Cryst. Growth* 233 (2001) 8-12.
- Z. Liu, D. Zhang, S. Han, C. Li, T. Tang, W. Jin, X. Liu, B. Lei and C. Zhou, *Adv. Mater.* 15 (2003) 1754-1757.
- Y. Chen, X. Cui, K. Zhang, D. Pan, S. Zhang, B. Wang and J. G. Hou, *Chem. Phys. Lett.* 369 (2003) 16-20.
- R. Z. Ma and Y. Bando, *Chem. Phys. Lett.* 370 (2003) 770-773.
- Y. Q. Zhu, W. K. Hsu, W. Z. Zhou, M. Terrones, H. W. Kroto and D. R. M. Walton, *Chem. Phys. Lett.* 347 (2001) 237-246.
- H. Y. Yang and T. W. Kim, *J. Ceram. Proc. Res.* 11 (2010) 769-772.
- C. S. Lim, J. H. Ryu, D.-H. Kim, S.-Y. Cho and W.-C. Oh, *J. Ceram. Proc. Res.* 11 (2010) 736-741.
- F. A. Sheikh, M. A. Kanjwai, H. Kim, D. R. Pandeya, S. T. Hong and H. Y. Kim, *J. Ceram. Proc. Res.* 11 (2010) 685-691.
- K.-S. Yun and C.-J. Park, *Electron. Mater. Lett.* 6 (2010) 173-176.
- C. Hong, H. Kim, H. W. Kim and C. Lee, *Met. Mater. Int.* 16 (2010) 311-315.
- H. W. Kim, H. S. Kim, M. A. Kebede, H. G. Na and J. C. Yang, *Met. Mater. Int.* 16 (2010) 77-81.
- Y.-S. Kim, K.-C. Kim and T.-W. Hong, *Met. Mater. Int.* 16 (2010) 225-228.
- D. Y. Lee, M.-H. Lee, N.-I. Cho, B.-Y. Kim and Y.-J. Oh, *Met. Mater. Int.* 16 (2010) 453-457.
- C. M. Choi, Y. C. Yoon, D. H. Hong, K. S. Brammer, K. B. Noh, Y. Oh, S. H. Oh, F. E. Talke and S. H. Jin, *Electron. Mater. Lett.* 6 (2010) 59-65.
- S. G. Shin, *Electron. Mater. Lett.* 6 (2010) 65-71.
- I.-S. Hwang, S.-J. Kim, J.-K. Choi, J. Choi, H. Ji, G.-T. Kim, G. Cao and J.-H. Lee, *Sens. Actuators B* 148 (2010) 595-600.
- M. Shahid, I. Shakir, S.-J. Yang and D. J. Kang, *Mater. Chem. Phys.* 124 (2010) 619-622.
- Y.-H. Lin, Y.-C. Hsueh, P.-S. Lee, C.-C. Wang, J.-R. Chen, J.-M. Wu, P.-P. Perng and H. C. Shih, *J. Electrochem. Soc.* 157 (2010) K206-K210.
- C. Jin, H. Kim, H.-Y. Ryu, H. W. Kim and C. Lee, *J. Phys. Chem. C* 115 (2011) 8513-8518.
- N. O. V. Plank, H. J. Snaith, C. Ducati, J. S. Bendall, L. Schmidt-Mende and M. E. Welland, *Nanotechnology* 19 (2008) 465603.
- X. Q. Meng, H. W. Peng, Y. Q. Gai and J. B. Li, *J. Phys. Chem. C* 114 (2010) 1467-1471.
- J. Bandara and U. W. Pradeep, *Thin Solid Films* 517 (2008) 952-956.
- J. Bandara and R. A. S. S. Ranasinghe, *Appl. Catal. A: General*

- 319 (2007) 58-63.
28. M. K. I. Senevirathna, P. K. D. D. P. Pitigala, E. V. A. Premalal, K. Tennakone, G. R. A. Kumara and A. Konno, *Sol. Energ. Mater. Sol. Cells* 91 (2007) 544-547.
29. H. S. Kim and H. W. Kim, *Act. Phys. Pol. A* (2009) 58-61.
30. H. W. Kim and N. H. Kim, *Appl. Surf. Sci.* 230 (2004) 301-306.
31. H. W. Kim and S. H. Shim, *Chem. Phys. Lett.* 422 (2006) 165-169.
32. S. H. Sun, G. W. Meng, G. X. Zhang, T. Gao, B. Y. Geng, L. D. Zhang and J. Zuo, *Chem. Phys. Lett.* 376 (2003) 103-107.
33. L. Abello, B. Bochu, A. Gaskov, S. Koudryavtseva, G. Lucazeau and M. Roumyantseva, *J. Solid State Chem.* 135 (1998) 78-85.
34. Y. Liu and M. Liu, *Adv. Funct. Mater.* 15 (2005) 57-62.
35. P. S. Peercy and B. Morosin, *Phys. Rev. B* 7 (1973) 2779-2786.
36. K. Ishikawa, N. Fujima and H. Komura, *J. Appl. Phys.* 57 (1985) 973-975.
37. H. K. Böckelmann and R. G. Schlecht, *Phys. Rev. B* 10 (1974) 5225-5231.
38. X. P. Peng, L. D. Zhang, G. W. Meng, Y. T. Tian, Y. Lin, B. Y. Geng and S. H. Sun, *J. Appl. Phys.* 93 (2003) 1760-1763.
39. J. Q. Hu, X. L. Ma, N. G. Shang, Z. Y. Xie, N. B. Wong, C. S. Lee and S. T. Lee, *J. Phys. Chem. B* 106 (2002) 3823-3826.
40. J. Q. Hu, Y. Bando, Q. Liu and D. Golberg, *Adv. Func. Mater.* 13, 493-496 (2003).
41. B. Cheng, J. M. Russell, W. Shi, L. Zhang and E. T. Samulski, *J. Am. Chem. Soc.* 126, 5972-5973 (2004).
42. H. W. Kim and S. H. Shim, *Appl. Phys. A* 88 (2007) 769-773.
43. H. W. Kim and S. H. Shim, *Chem. Phys. Lett.* 422 (2006) 165-169.
44. Ihsan Barin, Thermochemical data of pure substances, 3rd ed. (VCH, Weinheim, Germany, 1995).